Yajun Fan
Department of Mechanical Engineering,
Columbia University,
New York, NY 10027
e-mail: yf2121@columbia.edu

Zhishang Yang
Technical Center,
Caterpillar, Inc.,
Peoria, IL

Peng Cheng
Department of Mechanical Engineering,
Columbia University,
New York, NY 10027

Keith Egland
Technical Center,
Caterpillar, Inc.,
Peoria, IL

Lawrence Yao
Department of Mechanical Engineering,
Columbia University,
New York, NY 10027

Investigation of Effect of Phase Transformations on Mechanical Behavior of AISI 1010 Steel in Laser Forming

In laser forming, phase transformations in the heat affected zone take place under steep cooling rates and temperature gradients, and have a significant affect on the laser forming process and final mechanical properties of products. In this work, phase transformations during laser forming of AISI 1010 steel are experimentally and numerically investigated and the transient volume fraction of each available phase is calculated by coupling the thermal history from finite element analysis with a phase transformation kinetic model. Consequently, the flow stresses of material are obtained from the constitutive relationship of the phases, and the laser forming process is modeled considering the effect of work hardening, recrystallization and phase transformation. A series of carefully controlled experiments are also conducted to validate the theoretically predicted results. [DOI: 10.1115/1.2162911]

1 Introduction

Laser forming is a flexible forming process, during which a laser beam causes local thermal expansion, and deformation is obtained by non-uniform release of thermal stresses during cooling. In the past decades, great progress has been made in understanding the laser forming mechanisms [1,2] and in investigating the effects of important process parameters on the deformed shape and mechanical properties of the formed parts [3–6]. In particular, considerable research has been carried out on computer modeling of the laser forming process. However, the application of numerical modeling is limited by the lack of precise data of the temperature and strain rate dependent flow stresses of materials. In the past, the flow stress data were generally obtained by experiments, which were cumbersome, time consuming and whose methodology was case specific for different materials. More recently, several semi-empirical material models have been developed based on the knowledge of physical metallurgy of steel. For example, Pauskar and Shivpuri [7] provided the constitutive equations of Mn steel for flow stresses during hot rolling in which the effect of metallurgical phenomena such as strain hardening, dynamic recovery and recrystallization on flow stresses was considered, but the influence of phase transformation was neglected.

With very fast heating and cooling, laser forming is significantly different from other hot working processes. During laser forming, steep temperature gradients and thermal cycles cause severe microstructural changes in the heat affected zone (HAZ), and fairly high strain and strain rate are also involved; however, melting has to be avoided. Cheng and Yao [8] introduced the methodology of numerical modeling during normal hot working processes such as hot rolling into laser forming of AISI 1012 steel, and the flow behavior of material under steep thermal cycles was modeled considering strain hardening, dynamic recrystallization and phase transformations. The contribution of each phase to flow stresses under different stages, recovery or recrystallization, was calculated. The numerical results agreed very well with the experimental results. However, due to the complexity of the laser forming process and a lack of key material data, the phase transformations and the grain structural evolution occurring during the laser forming process were not fully investigated. Instead, some approximations were made. For example, the phase constitution during $\alpha \rightarrow \gamma$ phase transformation was simplified to be a linear relationship from A_{1ne} temperature to A_{3ne} temperature.

With recent developments in computer simulation of phase transformations and grain structural evolutions based on the fundamental kinetic and thermodynamic theories, it is possible to introduce these techniques to describe the particular laser forming process. In the present research, by combination of experiments and modeling, we seek to quantitatively understand the kinetics of phase transformation and grain structural evolution during laser forming of AISI 1010 steel and their influence on flow behavior and deformation (in particular, the $\alpha \rightarrow \gamma$ phase transformation during rapid heating, the decomposition of γ phase during rapid cooling, and the recrystallization). During rapid heating, the $\alpha \rightarrow \gamma$ phase transformation process can be modeled by a modified Johnson–Mehl–Avrami (JMA) equation for non-isothermal process. During cooling, the phase transformations are more complicated and involve not only the first order phase transformation but also displacive transformation. In this way, the JMA equation would not work to predict the phase transformation during cooling. The decomposition of γ phase during cooling in the welding process has been examined by Bhadeshia et al. [9–11]. Given the cooling rate, their model can provide a real time quantitative description of phase constitution in the heat affected zone. In our current research, Bhadeshia's phase transformation model [9–11] was applied to predict the phase transformation during cooling considering the similarity of thermal cycles in the HAZ caused by laser forming and welding. Then, using the same methodology provided by Cheng and Yao [8], the flow stress can be obtained in real time based on the phase constitution information, and the deformation can be predicted with an extensively tested thermal-mechanical finite element model [3,5,6,8].

Contributed by the Manufacturing Engineering Division of ASME for publication in the JOURNAL OF MANUFACTURING SCIENCE AND ENGINEERING. Manuscript received July 1, 2004; final manuscript received November 7, 2005. Review conducted by S. R. Schmid.

The objective of this work is to present a sequentially coupled thermal-microstructural—mechanical model to predict the deformation during complex laser forming processes. To validate the theoretically predicted results, a series of carefully controlled experiments are also conducted.

2 Mathematical Modeling

2.1 Flow Stress Modeling. During laser forming, phase transformations take place in the HAZ and each present phase also undergoes work hardening and softening of dynamic recovery and recrystallization. Therefore, the strategy to model flow behavior is to calculate the flow stress of each single phase, which is influenced by the dynamic recovery and recrystallization, and then sum up the contribution of each phase by the rule of mixtures

$$\sigma_{\text{total}} = \sum_{j=1}^{N} X_j \sigma_j \tag{1}$$

where σ_{total} is the total flow stress, and X_j and σ_j are the volume fraction and the flow stress of the jth phase of the material, respectively. The volume fraction X_j was determined by the phase transformation model, which will be introduced later.

When strain is less than the critical strain ε_c, only work hardening and dynamic recovery exist. The classical approach to model flow stress in the regime uses the following expression [12]

$$\sigma^{\text{rec}} = [\sigma_{\text{ss}}^{*2} + (\sigma_0^2 - \sigma_{\text{ss}}^{*2}) e^{-\Omega\varepsilon}]^{0.5} \tag{2}$$

where σ^{rec} represents the flow stress in the dynamic recovery regime, σ_0 is the initial stress, σ_{ss}^{*} is the imagined steady state stress when strain is infinite, Ω represents the ease of dynamic recovery and ε is the strain. The values of all the parameters for different phases and ε_c are adopted from the earlier paper [8].

The recrystallization takes place if the strain is larger than ε_c. The flow stress is calculated by the equation [8]

$$\sigma = \sigma^{\text{rec}} - [\sigma_{\text{ss}}^{*2} - \sigma_{\text{ss}}^{\text{rex}}]\left[1 - \exp\left(-K_d\left(\frac{\varepsilon - \varepsilon_c}{\varepsilon_{0.5} - \varepsilon_c}\right)^{n_1}\right)\right] \tag{3}$$

where $\sigma_{\text{ss}}^{\text{rex}}$ is the steady state stress after recrystallization has progressed through the material, $\varepsilon_{0.5}$ is the strain corresponding to 50% softening due to dynamic recystallization, and K_d and n_1 are constants. Similarly, the values of those parameters are obtained from Ref. [8].

2.2 Phase Transformation Modeling

2.2.1 $\alpha \rightarrow \gamma$ Transformation During Heating. In the rapid heating during laser forming, the $\alpha \rightarrow \gamma$ transformation in low alloy steels involves the nucleation of γ phase from the α matrix and the growth of γ phase by diffusion. Therefore, the JMA equation is applicable to describe the $\alpha \rightarrow \gamma$ transformation in AISI 1010 steel. This equation is expressed as [13]

$$f(t) = 1 - \exp[-(kt)^n] = 1 - \exp\left[-\left\{k\sum_{i=1}\Delta t_i\right\}^n\right] \tag{4}$$

where f stands for the transformed volume fraction of γ phase, t is the time, the JMA time exponent n is a constant independent of temperature and its value is determined by the nucleation and growth mechanism, Δt_i is time step of step i, and k is the rate factor and a function of temperature which can be calculated by the Arrhenius equation

$$k = k_0 \exp\left(-\frac{Q}{RT}\right) \tag{5}$$

where Q is the activation energy of the transformation, which does not change significantly with the variation of carbon and alloy concentrations, k_0 is the pre-exponential constant, R is the universal gas constant, and T is the absolute temperature. The temperature field and thermal cycles are calculated from the extensively tested FEM thermal modeling of laser forming. The values of constants Q, n, and k_0 have been used as 117.07 KJ mol^{-1}, 1.9, and 1.33×10^5, respectively, in the welding of AISI 1005 steel [14]. Considering the similarity of the material composition between AISI 1010 steel and 1005 steel as well as the insensitiveness to temperature of those parameters, these values were used in the present investigation.

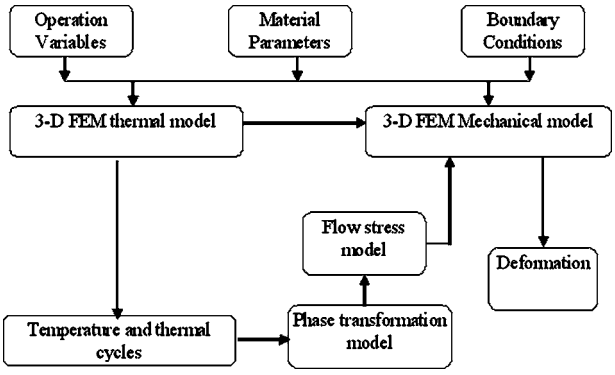

Fig. 1 Flow chart of the coupled thermal-microstructural-mechanical modeling approach

2.2.2 γ Phase Decomposition During Cooling. The γ phase decomposition during cooling was modeled by the phase transformation model provided by Bhadeshia [9–11]. In the model, the time-temperature-transformation (TTT) and continuous cooling transformation (CCT) diagrams were first calculated based on thermodynamics and phase transformation kinetics. Based on the calculated cooling rate, the produced phases and their volume fractions were then determined. The model can predict the phase transformations of not only Widmanstatten ferrite and allotriomorphic ferrite, but also pearlite, bainite, and martensite. The model's details [9–11,15,16], assumptions, salient features, and recent applications [14,17] are available in the literature.

Due to very high cooling rates in the involved cases, martensite may be the dominant phase after laser scanning. In Bhadeshia's model [9–11], the amount of martensite $V_{\alpha'}$ is calculated by an empirical formula [18]

$$V_{\alpha'} = (\mathbf{1} - V_M)[\mathbf{1} - \exp\{-\mathbf{0.011}(M_s - T)\}] \tag{6}$$

where M_s is the martensite start temperature and V_M is the volume fraction of microphases, which can be estimated as in Bhadeshia et al. [9,10].

3 Simulation and Experiments

3.1 Modeling Procedure. To systematically predict the laser forming process based on the coupled thermal-microstructural-mechanical modeling, the mathematical models described in the previous three sections need to be rationally arranged. Figure 1 shows the flow chart of the integration of these models.

The heating and deformation during laser forming are both symmetrical about the laser scanning path; therefore only half of the plate ($80 \times 40 \times 0.89$ mm^3) is modeled in the current research. More details about the sequentially coupled thermal-mechanical modeling of laser forming can be found in Refs. [3–6], in which the temperature dependent flow stress data came from experiments. The temperature field and thermal cycle are calculated from the 3D thermal finite element method (FEM) modeling, and then the calculated temperature is input into the phase transformation model to get the volume fraction of each phase at a given time step. Because the phase transformation model and grain evolution model require very fine grids to assure enough accuracy, all phase transformation and grain evolution simulations are only carried out on a cross section perpendicular to the scanning path of

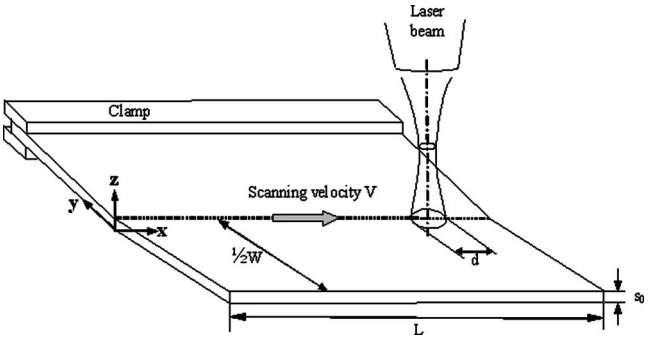

Fig. 2 Schematic of straight-line laser bending of AISI1010 steel sheet: s_0 is sheet thickness, W sheet width, L sheet length, and d laser spot diameter

the plate. This is reasonable considering that all points along the scanning direction undergo similar thermal cycles and deformations. The flow stresses are calculated based on the phase volume fractions from phase transformation modeling. Finally, the temperature field and flow stresses are input into the mechanical model to calculate the thermal strain and predict the deformation.

Two cases were run in the current research: $P=800$ W and $V=50$ mm/s, and $P=400$ W and $V=25$ mm/s, where P represents power and V is scanning velocity. In both cases, the laser beam spot size is 4 mm in diameter.

3.2 Experiment. To validate the theoretical models, a series of carefully controlled experiments were conducted. AISI 1010 steel plates of $80\times80\times0.89$ mm^3 were laser scanned straight along the center line under different conditions: 800 W and 50 mm/s and 400 W and 25 mm/s, maintaining spot size 4 mm diameter (Fig. 2). To enhance laser absorption by the plates, a graphite coating was applied to the surface exposed to the laser. The laser system used was a PRC 1.5 kW CO_2 laser with transmission electron microscopy TEM_{00} mode. After scanning, the bending angles of the formed plates were measured by a coordinate-measuring machine (CMM). The plates were cross sectioned perpendicular to the scanning path, polished and etched. The changes of macro and microstructures in the HAZ were observed under scanning electron microscopy (SEM). Finally, the Vickers microhardness was measured at points along the thickness of the HAZ on the scanning path.

4 Results and Analysis

4.1 Macro- and Microstructures From Experiments. Fig. 3 shows the SEM images of the laser formed cross section perpendicular to the scanning path. A distinctly darkened region is observed. The darkened subregion immediately below the top surface is the heat affected zone (HAZ), where phase transformation took place but no melting was involved. Because the HAZ experienced high temperature and deformation, significant recrystallization took place. Both recrystallization and phase transformation caused refined grains in the HAZ. In addition, different from most thermomechanical processes, the typical thermal cycle experienced during the laser forming was very steep, which meant that the time for grain growth was severely limited. As a result, the grains in the HAZ were visibly refined. Although the input line energy (P/V) was same for the two cases, the time for heat dissipation was longer with the faster scanning velocity. Thus, the case with the higher power and faster velocity (800 W and 50 mm/s) achieved a higher peak temperature and a larger HAZ.

Figure 4 shows the boundary of the HAZ under the conditions of 400 W and 25 mm/s. The boundary of the HAZ is clearly observed and the refined grains (around 10 μm) in the HAZ are much smaller than those (average 25 μm) in the base material. In the case of 800 W and 50 mm/s, the SEM imagines show similar

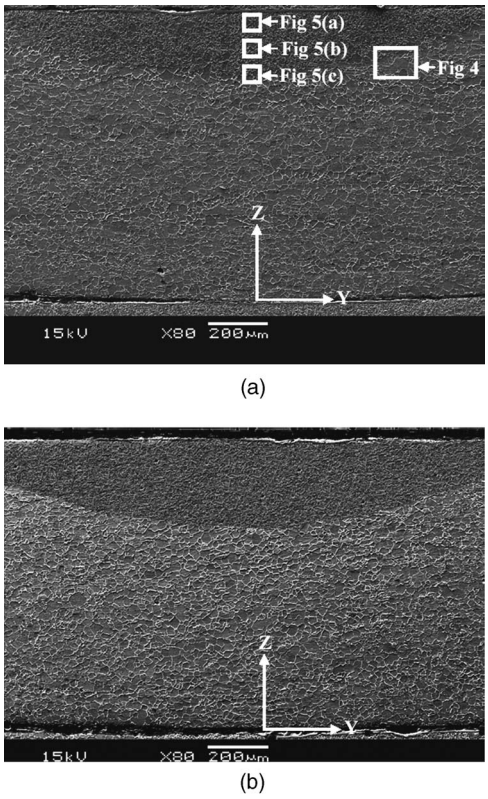

Fig. 3 The heat affected zone (HAZ) after laser scan, etched in 3% nital solution: (*a*) 400 W and 25 mm/s; (*b*) 800 W and 50 mm/s

results.

The phase morphology in the HAZ under the conditions of 400 W and 25 mm/s is shown by SEM imagines in Fig. 5. In Fig. 5(*a*), a large amount of different oriented packets with relatively parallel laths within them are observed, and the microstructure is considered as martensite Clearly, martensite is the dominant phase at the top of the HAZ, where the material experienced a very high cooling rate. Figure 5(*b*) shows that the martensite structure is still observed in the middle of the HAZ, but there exists a phase in the form of a small plate, different from retained austenite and martensite, remaining between lath martensite. This phase is thought to be the remained ferrite after the $\alpha\rightarrow\gamma$ transformation during heating. The observed area is in a zone with a mixture of martensite and retained ferrite. In Fig. 5(*c*), the remained ferrite plates become bigger and very little martensite in the form of small laths is observed. From the observation, in the bottom of the HAZ, the

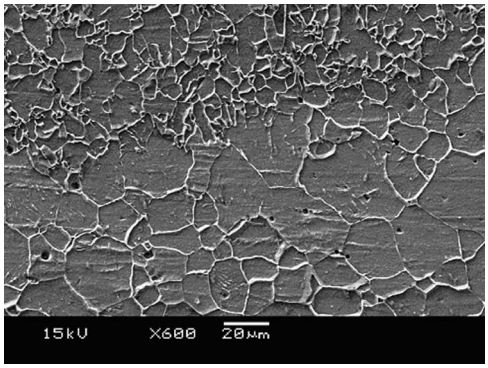

Fig. 4 The boundary of the HAZ at 400 W and 25 mm/s. The grain refinement in the HAZ can be observed.

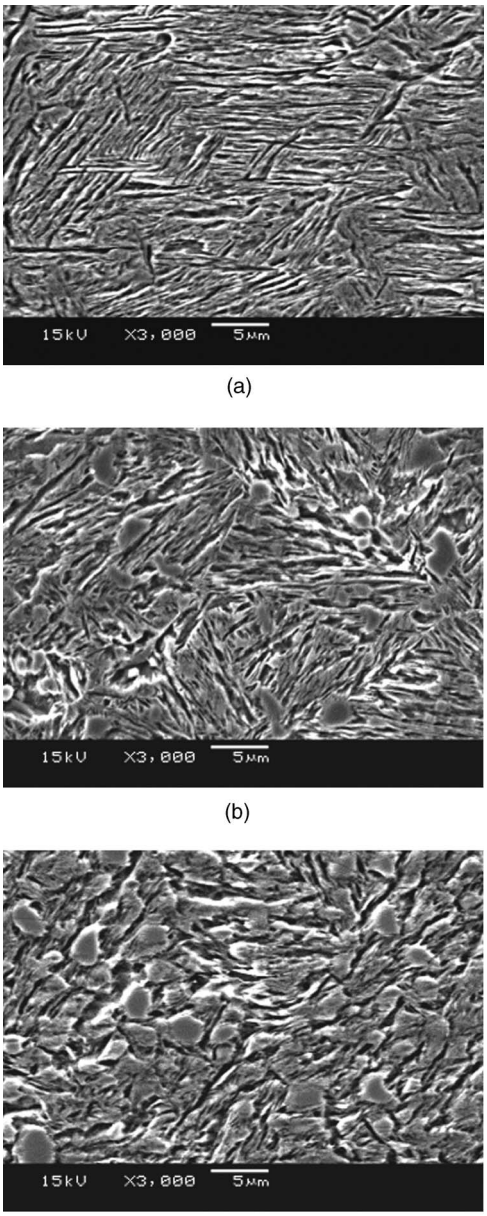

Fig. 5 Microstructural observations at different locations in the HAZ after laser scanning, 400 W and 25 mm/s: (*a*) top of the HAZ; (*b*) middle of the HAZ, and (*c*) bottom of the HAZ. Etched in saturated picral solution.

remained ferrite is the dominant phase. Based on the microstrutural observation at three typical locations in the HAZ, at the top, the predominant phase is martensite because in this area the peak temperature is above the nonequilibrium upper transformation temperature A_{3ne}, so the ferrite was completely transformed to austenite during heating, and then during cooling the austenite was transformed into martensite due to a very high cooling rate. In the middle of the HAZ, only part of ferrite was transformed into austenite during heating, so after cooling a mixture of remained ferrite and martensite was obtained. At the bottom, only very little of ferrite was transformed during heating, so the remained ferrite was the main phase after cooling. The case of 800 W and 50 mm/s also shows the same trend of phase distribution within the HAZ.

According to the experimental observation, the HAZ experienced significant recrystallization (the grain was evidently refined), and due to high cooling rate the martensite was substantially formed in the HAZ and the transformed austenite during heating was almost completely transformed to martensite after cooling.

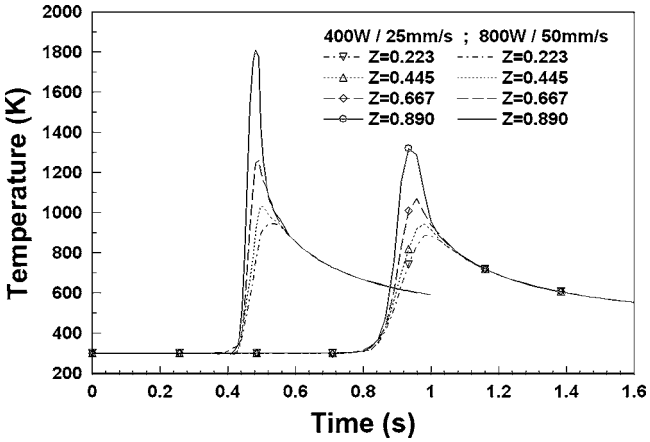

Fig. 6 The typical thermal cycles at different thickness depths on the scanning path (*X*=20 mm, *Y*=0 mm) from FEM thermal modeling of laser forming of AISI 1010 steel

4.2 Predictions by Modeling

4.2.1 Thermal Cycles. The calculated thermal cycles at different thickness depths on the scanning path are shown in Fig. 6. The figure shows that the heating rate and the cooling rate are very large, and the magnitude of heating rate is up to 1×10^5 K/s. The very rapid heating and cooling would cause considerable superheating and undercooling during the laser forming. For example, the melting temperature of AISI 1010 steel under equilibrium is about 1789 K, and the peak temperature in the case of 800 W and 50 mm/s is almost 1800 K, but due to superheating, melting was not observed from SEM imagines in this case. The final microstructure is also affected by the cooling rate within the austenite decomposition temperature range. During low cooling rate, which allows adequate time for the diffusion processes to occur, the product is equiaxed ferrite. As the cooling rates are increased, the austenite becomes inhomogeneous in composition, and then pearlite appears and grows into the austenite. Eventually, when the cooling rate become fast enough, bainite and martensite begin to form and, if the sample can be cooled fast enough, all of the diffusion-controlled transformations can be suppressed and only the martensitic transformation occurs. The critical cooling rate to form bainite is about 100 K/s for AISI 1010 steel [19], and from the thermal modeling, the transient cooling rate at the martensite start temperature M_s (about 780 K) is above 300 K/s. Therefore, almost all austenite is expected to form martensite during cooling, and bainite or pearlite are not produced.

4.2.2 Phase Transformations. The phase transformation during heating is relatively simple because no melting is involved and only the $\alpha\rightarrow\gamma$ transformation is considered. The process can be predicted by the JMA equation. When the heating process has just finished and the cooling process is about to start, which is assumed to be when the point at the top surface on the scanning path reaches its peak temperature, the calculated volume fractions of ferrite and transformed austenite are taken as the initial conditions for phase transformation prediction during cooling. On slow heating, the dissolution of carbides and the formation of the γ phase take place at about 997 K for AISI 1010 steel, producing a mixture of α and γ. The α phase transforms completely to γ at about 1120 K. There is a dual phase region from 997 to 1120 K. For the laser forming process, the dual phase region still exists, but the temperature range will shift up a little due to superheating. The

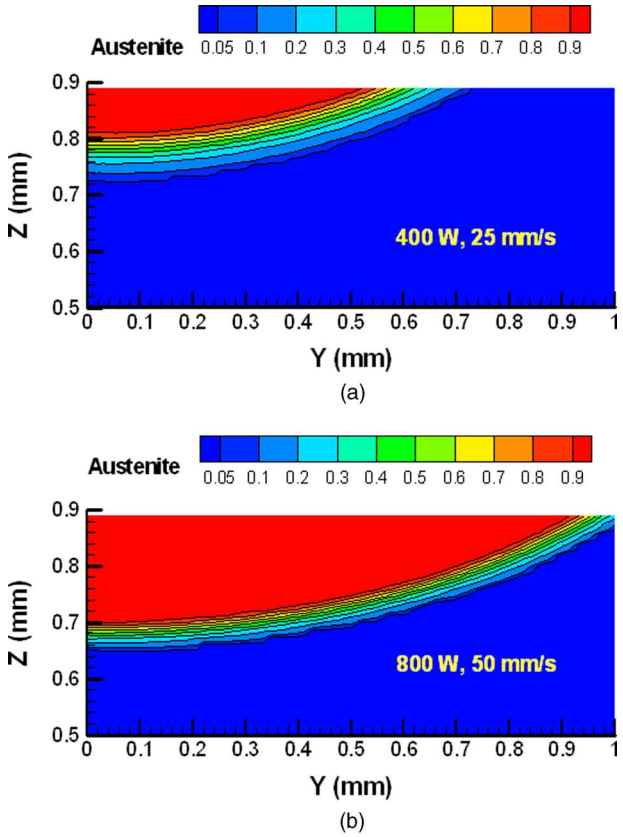

Fig. 7 The volume fraction of transformed austenite at the end of heating: (*a*) *P*=400 W, *V*=25 mm/s; and (*b*) *P*=800 W, *V*=50 mm/s

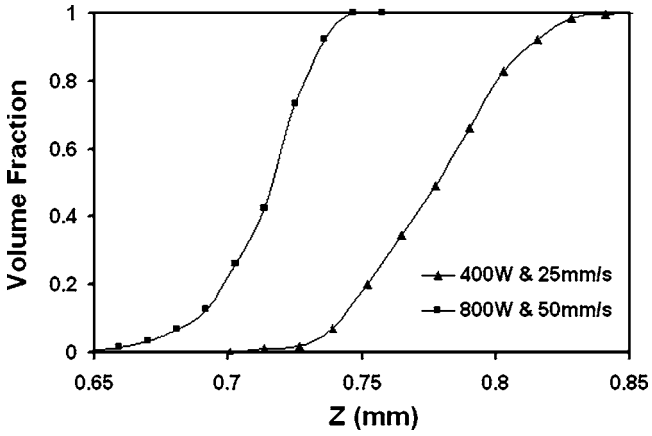

Fig. 8 The transformed austenite distribution at the end of heating along the thickness on the scan path (*Y*=0 mm)

calculated austenite phase distributions at the end of the heating process for both cases are shown in Fig. 7. The contours in Fig. 7 show that the HAZ region in the case of 800 W and 50 mm/s is larger than that in the case of 400 W and 25 mm/s, the same result as that of the SEM imagines. The comparison between the experimentally obtained and the calculated HAZ size is also given in Table 1. The comparison shows that the numerical result is in agreement with the experimentally obtained HAZ size.

To ensure that the values of the given material's parameters could produce the correct shapes of the γ fraction versus distance plot, the calculated distribution of transformed austenite along the thickness on the scan path was plotted in Fig. 8. The figure shows the exact exponential relationship between the phase fraction and the distance. Figure 8 also shows that the dual phase region in the case of 800 W and 50 mm/s is smaller than the 400 W and 25 mm/s case although the HAZ size is larger. In the case of 800 W and 50 mm/s, the time for heat dissipation is limited due to the faster scanning velocity and higher temperature gradient than in the case of 400 W and 25 mm/s. The larger temperature gradient also causes a smaller dual phase region in the case of 800 W and 50 mm/s.

The phase transformation during cooling is a process of the γ phase decomposition, and the products are dependent on cooling rate. To quantitatively predict the decomposition of the γ phase in the HAZ during cooling, the cooling rates calculated from the 3D FEM thermal modeling were coupled with the Bhadeshia phase transformation model [9–11]. The model was initially applied to predict the phase transformation during welding of low carbon steel. In the present research, it also worked well in the laser forming having steeper thermal cycles than the welding process. In the model, based on thermodynamics and phase transformation kinetics, the TTT and CCT diagrams and the volume fractions of the HAZ microstructures can be calculated using the given thermal history. The calculated phase distribution after laser forming in the conditions of 400 W and 25 mm/s is given in Fig. 9. From Fig. 9, almost all austenite was transformed to martensite under the very high cooling rate, and after heating the remained ferrite in the dual phase region is still there. The rest is the small amount of retained austenite (up to 3%). As we know, the martensitic transformation can never be complete; that is, a small amount of austenite is always retained. When the carbon content of steel is high and the M_s temperature is low, a larger volume fraction of retained austenite is obtained. For AISI 1010 steel, due to its very low carbon content, only films of inter-lath austenite are retained at room temperature. The quantity of retained austenite for low carbon steel is below 4%. The calculated phase distribution after cooling shows a similar trend to the experimental observation: at the top of the HAZ, martensite is predominant; in the middle, the mixture of martensite, remained ferrite and very little retained austenite (which cannot be observed from SEM images) is obtained; and at the bottom, the main phase is the remained ferrite. Similar numerical results are obtained in the case of 800 W and 50 mm/s. Figure 10 shows the measured Vickers microhardness at various thickness depths on the scanning path. From Fig. 10, the microhardness gradually decreases down from the top of the HAZ, and there is a steep drop at the bottom of the HAZ. Hardness in the HAZ was influenced by both phase constitution and work hardening. Martensite is the phase with very high hardness, and because the volume fraction of martensite drops quickly to zero in the dual phase region, an evident drop of microhardness at

Table 1 Comparison of HAZ size between experimental and numerical results

	HAZ depth (mm)		HAZ half width (mm)	
	Experimental	Numerical	Experimental	Numerical
400 W and 25 mm/s	0.20	0.19	0.78	0.74
800 W and 50 mm/s	0.27	0.25	0.95	1.02

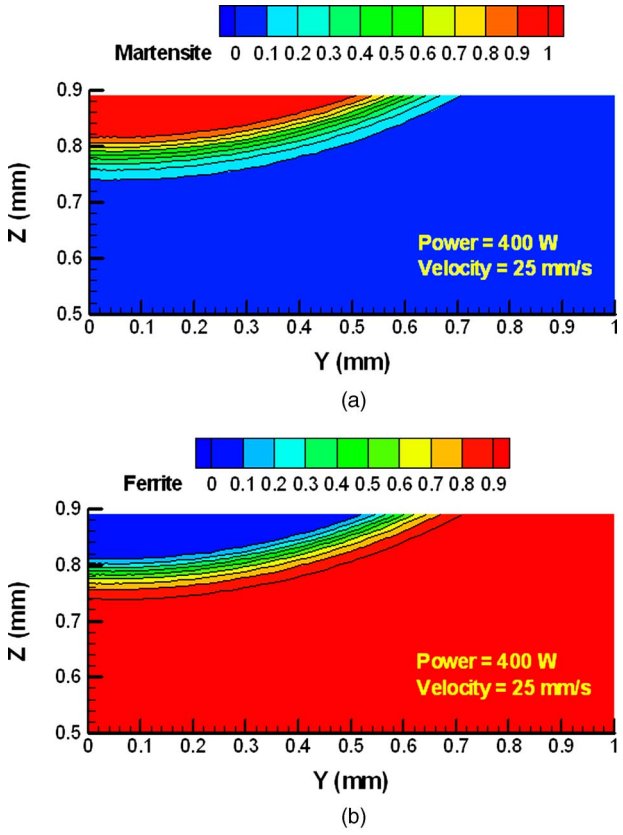

Fig. 9 The phase constitution after cooling, P=400 W, V =25 mm/s: (*a*) martensite and (*b*) ferrite

the bottom of the HAZ (the dual phase region) was observed. Above the dual phase region, martensite is the dominant phase, but the region closer to the top surface experienced higher peak temperature and larger plastic deformation, and thus, has a higher hardness due to work hardening. This also provides experimental evidence for the simulated phase distribution after cooling.

4.2.3 Deformations. After the real time phase constitutive information is obtained by the phase transformation modeling, the flow behavior can be calculated by the rule of mixtures (Eq. (1)).

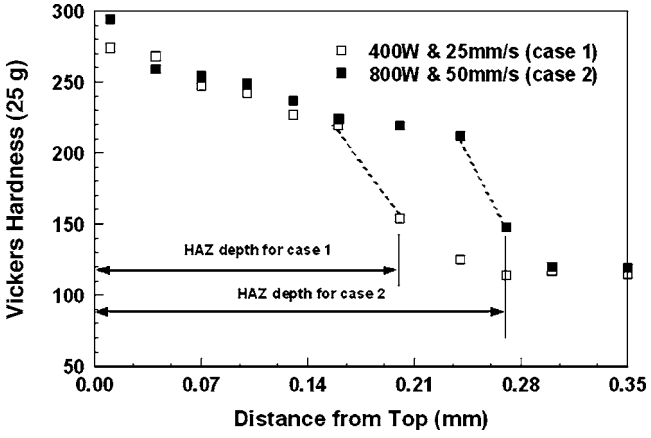

Fig. 10 The measured Vickers microhardness along thickness on the scanning path (Y=0 mm): test load=25 g and duration time=10 s. An evident hardness drop is in the bottom of the HAZ, where the volume fraction of martensite drops quickly to zero.

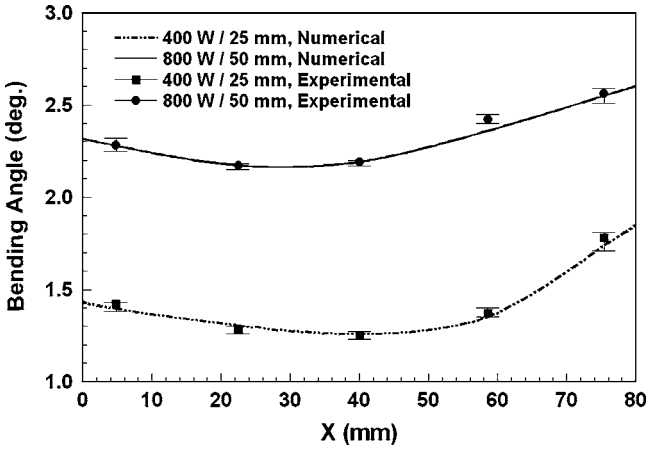

Fig. 11 The comparison between numerically predicted bending angles and experimentally obtained bending angles at various locations along scanning path (Y=0 mm)

Based on the calculated transient flow stress and the FEM mechanical modeling of laser forming, the bending angles of the plates can be predicted. Figure 11 shows that both the experimental and the numerical results of the bending angle along the scanning path agree with each other very well. It can be seen that, from the entering end of the scanning path (X=0 mm), the bending angle first drops a little and then increases to a greater angle at the exiting end. This phenomenon is called the edge effect and was already investigated in detail in an earlier research [4]. The drop of the bending angle after the laser enters the plate is caused by the stronger surrounding constraint in the middle of the plate. The bending edge curvature is dependent on the bending mechanism, constraint by the surrounding material and preheating. In the 400 W and 25 mm/s case, due to its slower scanning velocity, the exiting end was preheated to a fuller extent. Therefore, when the heat source moved from the entering end to the exiting end, the increase of the peak temperature and the thermal expansion was larger. As a result, the increase of the bending angle in the exiting end was larger than that of the 800 W and 50 mm/s case. Also, the bending edge curvature in the case of 400 W and 25 mm/s was larger.

Figure 12 shows the simulated history of the Y component of the plastic strain at different points along the thickness on the scanning path. As seen, the plastic strain is severely compressive at the top surface of the plate and slightly compressive on the

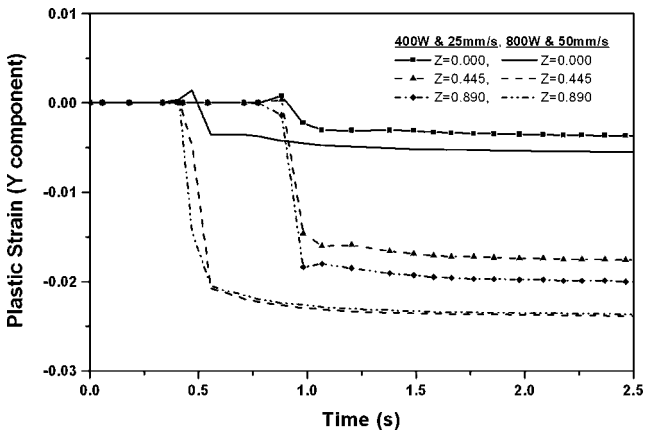

Fig. 12 Y-component of plastic strain along thickness on the scanning path (X=20 mm and Y=0 mm) from FEM mechanical modeling of laser forming of AISI 1010 steel

lower surface. These results are easily understood. During heating, both the top and bottom of the plate tended to thermally expand, but the thermal expansion was restricted by the surrounding material, which led to the compressive plastic strain at the stage of cooling. The top was heated to a higher temperature, and had a stronger tendency to expand; therefore, more compressive plastic strain was produced due to the restriction from the surrounding material, which makes the plate bend towards the laser.

5 Conclusions

A coupled thermal-microstructural-mechanical model has been developed for the laser forming process. The model considers the effect of phase transformation, work hardening, dynamic recovery and recrystallization on the deformation occurring during the laser forming process. The phase transformation of AISI 1010 steel during heating was modeled by the modified JMA equation, and the austenite decomposition during cooling was predicted by the Bhadeshia's phase transformation model, which was initially applied in the welding process. All the numerical results agree well with the experimental results.

The simulation and direct observations of the microstructure and deformation lead to the following conclusions:

(1) Under typical thin plate laser forming, a substantial amount of martensite is formed due to the extremely high cooling rate present after the laser scan.

(2) Due to phase transformation and significant recrystallization caused by high temperature and deformation in the HAZ, the grain is distinctly refined.

(3) According to comparison of the HAZ macrostructure, phase constitution and bending angle between the experimental and numerical results, the proposed coupled model is able to predict the microstructure evolution and the deformation caused through laser forming.

Acknowledgment

The authors acknowledge the financial support from NIST under Grant No. ATP-00005269. The authors thank Dr. Judson Marte and Dr. Micheal Graham of General Electric Global Research Center, and Professor Said Nourbakhsh, Polytechnic University, for the great help in the microhardness measurements. Helpful discussions with Dr. Marshall Jones from General Electric Global Research Center, and Dr. Jerry Jones from N.A. Technology are gratefully acknowledged.

References

[1] Vollertsen, F., 1994, "Mechanism and Models for Laser Forming," *Proceedings of LANE'94*, Sec. B, 1, Meisenbach Bamberg, Germany, pp. 345–360.
[2] Holzer, S., Arnet, H., and Geiger, M., 1994, "Extending Laser Bending for the Generation of Convex Shapes," *Proceedings of LANE'94*, Sec. B, 1, Meisenbach Bamberg, Germany, pp. 379–386.
[3] Li, W., and Yao, Y. L., 2000, "Numerical and Experimental Study of Strain Rate Effects in Laser Forming," ASME J. Manuf. Sci. Eng., **122**(3), pp. 445–451.
[4] Bao, J., and Yao, Y. L., 1999, "Study of Edge Effects in Laser Bending," Symposium on Advances in Laser Forming, *Proceeding ASME IMECE 1999*, Nashville, TN, ASME, New York, Vol. MED-10, pp. 941–948.
[5] Li, W., and Yao, Y. L., 2001, "Laser Bending of Tubes: Mechanism, Analysis and Prediction," ASME J. Manuf. Sci. Eng., **123**(11), pp. 674–681.
[6] Cheng, J., and Yao, Y. L., 2001, "Cooling Effects in Multiscan Laser Forming," J. Manuf. Process., **3**(1), pp. 60–72.
[7] Pauskar, P., and Shivpuri, R., 1999, "A Microstructure Dependent Flow Stress Model," Trans. North Am. Manuf. Res. Inst. SME, **XXVII**, pp. 67–72.
[8] Cheng, J., and Yao, Y. L., 2002, "Microstructure Integrated Modeling of Multiscan Laser Forming," ASME J. Manuf. Sci. Eng., **124**, pp. 379–388.
[9] Bhadeshia, H. K. D. H., and Svensson, L.-E., 1993, "Modelling the Evolution of Microstructure in Steel Weld Metal," *Mathematical Modeling of Weld Phenomena*, H. Cerjak and K. E. Easterling, eds., Institute of Materials, pp. 109–182.
[10] Bhadeshia, H. K. D. H., 1990, "Modelling the Microstructure in the Fusion Zone of Steel Weld Deposits," *Recent Trends in Welding Science and Technology*, S. A. David and J. M. Vitek, eds., ASM International, Materials Park, OH, pp. 189–198.
[11] Bhadeshia, H. K. D. H., Svensson, L.-E., and Gretoft, B., 1985, "Model for the Development of Microstructure in Low-Alloy Steel (Fe–Mn–Si–C) Weld Deposits," Acta Metall., **33**, pp. 1271–1283.
[12] Harford, W. F., and Caddle, R. M., 1983, *Metal Forming-Mechanics and Metallurgy*, Prentice–Hall, Englewood Cliffs, NJ.
[13] Johnson, W. A., and Mehl, R. F., 1939, "Reaction Kinetics in Processes of Nucleation and Growth," Trans. Am. Inst. Min., Metall. Pet. Eng., **135**, pp. 416–441.
[14] Zhang, W., Elmer, J. W., and DebRoy, T., 2002, "Modeling and Real Time Mapping of Phases During GTA Welding of 1005 Steel," Mater. Sci. Eng., A, **A333**, pp. 320–325.
[15] Bhadeshia, H. K. D. H., and Christian, J. W., 1989, "Bainite in Steels," Metall. Trans. A, **20A**(6), pp. 1037–1054.
[16] Takahashi, M., Bhadeshia, H. K. D. H., 1991, "Model for the Microstructure of Some Advanced Bainitic Steel," Mater. Trans., JIM, **32**, pp. 689–696.
[17] Calvo, F. A., Bently, K. P., and Baker, R. G., 1963, *Studies of the Welding Metallurgy of Steels*, BWRA, Abingdon, Cambridge, UK, p. 71.
[18] Trivedi, R., 1970, "Growth of Dendritic Needles From a Supercooled Melt," Acta Metall., **18**(3), pp. 287–296.
[19] Boyer, H. E., and Gray, A. G., eds., 1977, *Atlas of Isothermal Transformation and Cooling Transformation Diagrams*, ASM International, Materials Park, OH.